Mon. Not. R. Astron. Soc. **000**, 1–?? (2013) Printed 17 December 2013 (MN LATEX style file v2.2)

Impact of thermal diffusion and other abundance anomalies on cosmological uses of galaxy clusters

P. Medvedev[1⋆], M. Gilfanov[1,2], S. Sazonov[1,3], P. Shtykovskiy[1]
[1] *Space Research Institute, Russian Academy of Sciences, Profsoyuznaya 84/32, 117997 Moscow, Russia*
[2] *Max-Planck-Institut für Astrophysik, Karl-Schwarzschild-Str. 1, D-85741 Garching bei München, Germany*
[3] *Moscow Institute of Physics and Technology, 9 Institutsky per., 141700 Dolgoprudny, Moscow Region, Russia*

Aug. 2013

ABSTRACT

Depending on the topology of the magnetic field and characteristics of turbulent motions, diffusion can significantly affect the distribution of elements, in particular helium, in the intracluster medium (ICM). As has been noted previously, an incorrect assumption about the helium abundance will lead to an error in the iron abundance determined from X-ray spectroscopy. The corresponding effect on the temperature measurement is negligibly small. An incorrectly assumed helium abundance will also lead to a systematic error in angular distance measurements based on X-ray and Sunyaev–Zeldovich (SZ) observations of clusters of galaxies. Its magnitude is further amplified by the associated error in the metal abundance determination, the impact being larger at lower ICM temperatures. Overall, a factor of 2–5 error in the helium abundance will lead to an $\approx$ 10–25% error in the angular distance.

We solve the full set of Burgers equations for a multi-component intracluster plasma to determine the maximal effect of diffusion on the interpretation of X-ray and microwave observations of clusters of galaxies. For an isothermal cluster, gravitational sedimentation can lead to up to a factor of $\sim$ 5–10 enhancements of helium and metal abundances in the cluster center on a $\sim$ 3–7 Gyr timescale. In cool-core clusters on the contrary, thermal diffusion can counteract gravitational sedimentation and effectively remove helium and metals from the cluster inner core. In either case, a significant, up to $\approx$ 40%, error in the metal abundances determined by means of X-ray spectroscopy is possible. The angular distance determined from X-ray and SZ data can be underestimated by up to $\approx$ 10–25%.

Key words: X-rays: galaxy clusters. Cosmic microwave background. Intergalactic medium. Distance scale.

1 INTRODUCTION

Clusters of galaxies are an important tool of observational cosmology. The key role in fulfilling their potential as cosmological probes belongs to X-ray observations. X-ray imaging and spectroscopy, combined with the assumptions of hydrostatic equilibrium, symmetry and uniformity, yield the total gravitating masses of clusters of galaxies and their gas fractions. Another opportunity for cosmological measurements with clusters of galaxies is provided by the Sunyaev–Zeldovich (SZ) effect (Sunyaev & Zeldovich 1972). New-generation space- and ground-based SZ experiments, such as Planck, SPT, ACT and CARMA, are capable of mesuring electron pressure in the intracluster medium (ICM) independently of X-ray data (e.g. Plagge et al. 2010; Reese et al. 2012; Plagge et al. 2012; Planck Collaboration, et al. 2013). Combined observations in the microwave and X-ray bands allow one to measure the angular distances to clusters of galaxies and thus to determine the Hubble constant (Silk & White 1978; Sunyaev & Zeldovich 1980; Carlstrom et al. 2002; Motl et al. 2005; Bonamente et al. 2006; Kravtsov et al. 2006; Planck Collaboration, et al. 2012).

Interpretation of X-ray and SZ observations of clusters of galaxies is subject to a number of uncertainties. The nature of many (but not all) of these uncertainties are related to the physical state of the ICM, for example to the assumptions of hydrostatic equilibrium or symmetries in the ICM distribution, the role of non-thermal pressure, abundance distributions of elements etc. Many of these uncertain-

⋆ E-mail: tomedvedev@iki.rssi.ru

ties have been extensively discussed and are taken into account by sophisticated data interpretation procedures (e.g. Bonamente et al. (2006)). However, the effects of possible non-solar abundance distributions of elements remained so far largely ignored.

Diagnostics of element abundances in the ICM is based on measurement of their line emission, which, given the characteristic ICM temperatures, is in the X-ray band. This works reasonably well in principle for most of the cosmically abundant elements. However, X-ray spectroscopy provides no information on the helium-to-hydrogen ratio in the ICM, because both elements are fully ionized at these temperatures and produce no spectral lines. Therefore in practice, the helium abundance is usually assumed to be equal to its primordial value. The latter is known quite accurately from the theory of Big Bang nucleosynthesis which predicts the He fraction in the total baryonic mass density of $Y = 0.2482 \pm 0.0007$ (Walker et al. 1991; Kneller & Steigman 2004). However, abundances of elements in the ICM may differ significantly from the primordial values. It has been shown that sedimentation of helium and heavy elements (Fabian & Pringle 1977; Gilfanov & Sunyaev 1984; Chuzhoy & Nusser 2003; Chuzhoy & Loeb 2004; Ettori & Fabian 2006; Shtykovskiy & Gilfanov 2010) may take place in the central regions of clusters. If transport processes are not significantly suppressed in the ICM, helium abundance may increase by a factor of 2 or more in the cluster center. For comparison, helium enrichment by stars is not expected to be significant.

An incorrect assumption about helium abundance in interpreting observations of clusters of galaxies will lead to several important consequences. Firstly, the incorrect calculation of the continuum level, per particle, will result in an incorrect measurement of the metal abundances and emission measures by means of X-ray spectroscopy (Drake 1998; Ettori & Fabian 2006). That in turn will result in incorrect estimates of the gravitating and gas masses of the cluster (Ettori & Fabian 2006). Secondly, incorrectly assumed helium abundance will affect the results of angular distance measurements based on X-ray and microwave observations (Markevitch 2007; Bulbul et al. 2011).

Although different aspects of the helium abundance problem have already been discussed, the amplitude of its effects having been estimated and their potential importance for cosmological measurements with clusters of galaxies stressed out, none of the previous treatments included the full consideration of the diffusion problem. In particular, the effect of thermal diffusion was not taken into account. The importance of the latter in considering cool-core clusters has been demonstrated by Shtykovskiy & Gilfanov (2010). In particular, it was shown that the temperature gradients in cool-core clusters are large enough for thermal diffusion to counteract gravitational sedimentation and to reverse the flow of heavy particles, resulting in the effective removal of helium and metals from the cluster inner core.

The goal of the present paper is to consider the full set of Burgers equations for a multi-component ICM plasma in order to estimate the maximum possible impact of diffusion of elements in the ICM on the interpretation of X-ray and microwave observations of clusters of galaxies. In the following we will consider both isothermal and cool-core clusters. As a representative example of a cool-core cluster we will use Abell 2029. The paper is organized as follows. In Section 2, we revisit the problem of bias in the observationally derived ICM parameters caused by incorrectly assumed helium abundance. In Section 3, we describe our treatment of the diffusion problem and present the results of computations for A2029 and an isothermal cluster of the same mass. Finally, in Section 4 we discuss implications of our results for observational cosmology.

2 BIAS IN X-RAY AND SZ DERIVED QUANTITIES DUE TO INCORRECTLY ASSUMED HELIUM ABUNDANCE

For a spherically symmetric gas distribution, the X-ray surface brightness in the direction of the cluster center is given by:

$$S_x = \frac{2}{4\pi(1+z)^4} D_a \int\limits_0^{\theta_c} n_e^2(\theta)\Lambda(A(\theta), T_e(\theta)) d\,\theta. \quad (1)$$

Here, z and D_a are the cluster redshift and angular distance, respectively, $n_e(\theta)$ and $T_e(\theta)$ are the electron number density and temperature at distance $r = D_a\theta$ from the cluster center along the line of sight, Λ is the X-ray cooling function of the ICM integrated over a given energy band, and θ_c is the cluster angular size. Note that we define Λ relative to n_e^2.

The amplitude of the nonrelativistic Sunyaev–Zeldovich effect is proportional to the Comptonization parameter. The Comptonization parameter for the same (central) line of sight as in equation (1) is given by (Sunyaev & Zeldovich 1972)

$$y = 2D_a \frac{k\sigma_T}{m_e c^2} \int\limits_0^{\theta_c} T_e(\theta) n_e(\theta) d\,\theta, \quad (2)$$

where m_e, c, σ_T, k are the electron mass, speed of light, Thomson cross section and Boltzmann's constant, respectively.

2.1 X-ray derived quantities

At typical ICM temperatures of $T \sim 10^7$–10^8 K, hydrogen and helium are fully ionized and radiate mostly by bremsstrahlung. Hence, the helium abundance cannot be determined directly from X-ray observations. Analyzing the X-ray spectrum of the ICM, an observer has to make some assumptions about the helium–hydrogen ratio in order to determine the abundances of heavy elements and the temperature and density of the gas.

To estimate the bias in these quantities caused by an incorrect assumption about helium abundance, we carried out the following simulations. Using the VAPEC model (Smith et al. 2001) in XSPEC (Arnaud 1996), we generated X-ray spectra for different gas temperatures, fixing the abundances of heavy elements to their solar values and varying the helium abundance from 0.1 to 2 in solar abundance units. The simulated spectrum was then fit by the same model with the helium abundance fixed at the solar

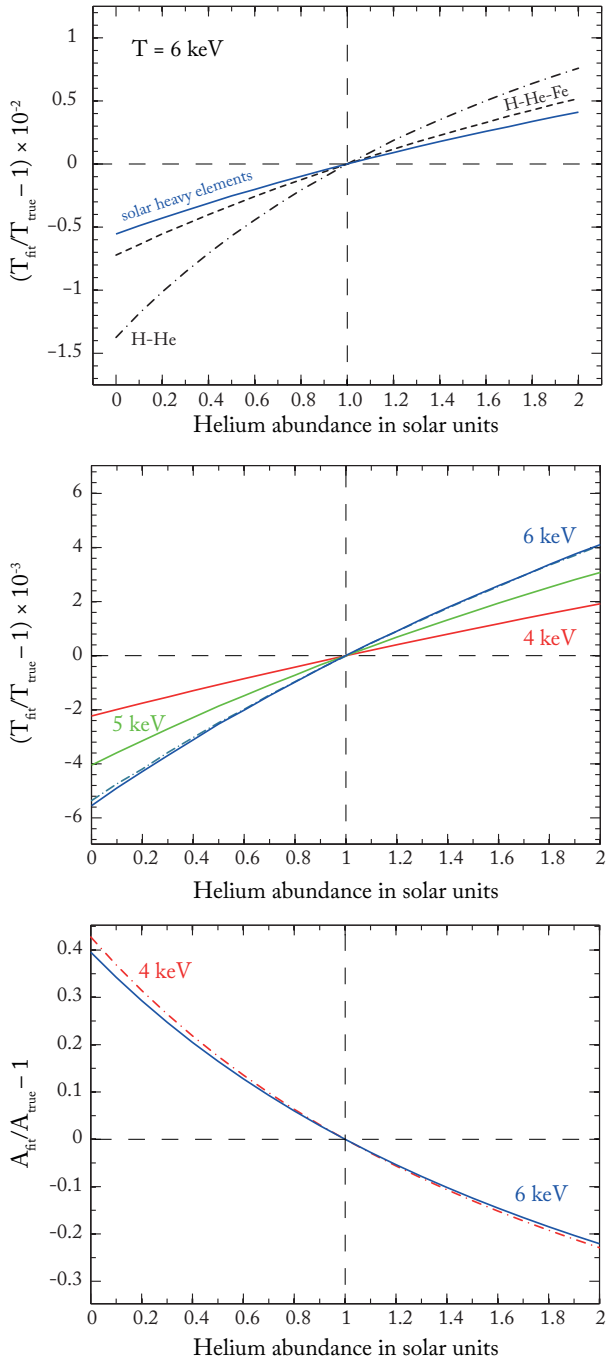

Figure 1. Bias in the determination of the temperature (top and middle panels) and metal abundance (bottom) as a function of the helium abundance. The helium abundance was assumed to be solar in spectral fitting. *Top:* Temperature bias for gas with $kT = 6$ keV and different compositions: solar abundances of elements heavier than helium (blue solid line); plasma consisting of H, He and solar-abundance Fe (black dashed line); H–He plasma (black dash-dotted line). *Middle:* Temperature bias for gas with solar abundances of elements heavier than helium and different temperatures: 4 (red), 5 (green) and 6 (blue) keV. The blue dash-dotted line corresponds to the bias for spectra generated with the XMM-Newton instrumental response ($T = 6$ keV). *Bottom:* Bias in the metal abundance determination for gas with solar abundances of elements heavier than helium and temperatures of 4 (red) and 6 (blue) keV.

value and other element abundances characterized by a single number z — the abundance ratio to the solar value, which, along with the temperature, were free parameters of the fit. In the simulations and spectral fitting, the Chandra (ACIS-I3 Cycle 15) response was used; the spectral fitting was performed in the 0.5–10 keV energy band. Poisson noise was not included in simulated spectra.

The results of these calculations are presented in Fig. 1. In the top and middle panels, we compare the bias in the determination of temperature for plasmas of different composition and temperature. The bias is significantly stronger in the case of pure H–He plasma compared to gas enriched by metals and increases with temperature. However, its overall amplitude is negligibly small, less than 1%. Replacing the Chandra response function with that of XMM-Newton EPIC MOS has practically no effect on this result. Hence, the error in the helium abundance assumption does not significantly affect the determination of gas temperature. This can be explained by the fact that the inferred gas temperature is determined by the shape of the spectral continuum and relative intensities of spectral lines. Changing the helium abundance affects the continuum shape only slightly because the energy dependence of the Gaunt factor weakly varies with the ion charge Z (see, e.g., Hummer 1988), so that hydrogen and helium have only slightly different shapes of bremsstrahlung spectra.

In the bottom panel of Fig. 1, we show the relative error in the determination of heavy element abundances as a function of the true helium abundance for different gas temperatures. The error in the determination of heavy element abundances resulting from the assumption of solar helium abundance can reach $\sim 40\%$ if the true helium abundance is zero. For a factor of 2 error in the assumed helium abundance, the error on the heavy element abundances is about $\approx 20\%$. Similar results were previously obtained by Drake (1998); Ettori & Fabian (2006). The error in the heavy element abundances arises because, due to incorrectly assumed helium abundance, the spectral model incorrectly calculates the continuum level per hydrogen atom, which affects the ratio of the emission line intensities to the continuum. As increasing helium abundance leads to increasing the continuum level per particle, the heavy element abundances are underestimated when the helium abundance is underestimated. The effect depends weakly on the gas temperature, being larger for lower temperatures.

2.2 Angular distance

The X-ray brightness and SZ decrement depend on different powers of the electron density. Therefore, a combination of X-ray and SZ observations provides an opportunity to determine this density and convert it to the cluster distance using equations (1) and (2) (Silk & White 1978; Sunyaev & Zeldovich 1980):

$$D_a = \frac{y^2}{S_x} \frac{\int\limits_0^{\theta_c} n_e^2 \, \Lambda d\theta}{\left(\int\limits_0^{\theta_c} n_e \, T_e d\theta \right)^2} \frac{m_e^2 c^4}{2k^2 \sigma_T^2 4\pi (1+z)^4}, \qquad (3)$$

where y and S_x are the Comptonization parameter (determined from the observed SZ decrement) and X-ray surface

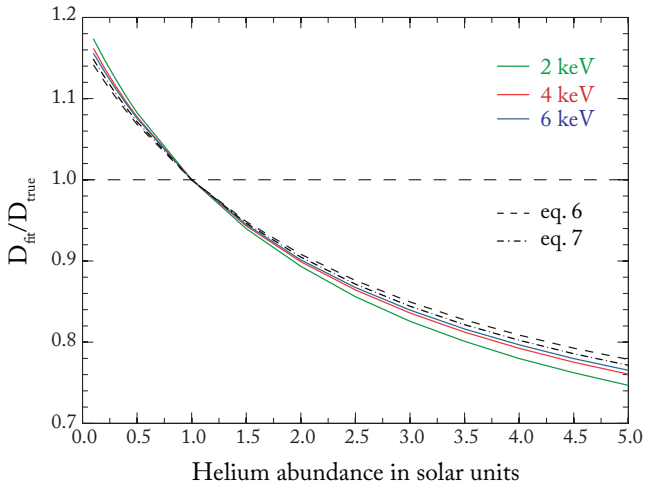

Figure 2. The bias in the distance to a uniform cloud of hot plasma derived from a combination of SZ and X-ray (Chandra) data, as a function of helium abundance. In the simulated data, the abundances of all elements heavier than helium were set equal to their solar values. The simulated data were interpreted assuming solar helium abundance, whereas the abundances of heavy elements were determined from X-ray spectral fitting. The green, red and blue solid lines show the distance bias computed using the precise expression, eq. (4), for the plasma temperature of 2, 4 and 6 keV. For comparison, the black dashed and dash-doted lines show the bias for H–He plasma derived from the precise expression, eq. (6), and approximate relation, eq. (7), respectively.

brightness, both measured in the direction towards the cluster center. Whereas both y and S_X are directly measured quantities, the radial temperature profile $T(\theta)$ and the shape of the density profile $n_e(\theta)$ can be inferred from observations, e.g., from the radial brightness profiles in different X-ray bands. Note that in order to determine the normalization of $n_e(\theta)$ one would need to know the distance to the cluster, however, the density normalization is not required for the angular distance calculation as it cancels out in eq.3. The cooling function Λ depends, apart from the temperature T, on the assumed helium abundance x and metal abundances z, the latter usually being determined from X-ray spectral fitting, i.e. $\Lambda = \Lambda(x, z, T)$. Note that the cooling function is normalized to the square of electron density n_e^2.

To investigate how distance measurements can be affected by an error in the assumed helium abundance, we considered an isothermal spherical gas cloud of constant density and homogeneous chemical composition with an angular size of θ_c located at distance D_a^{true} from the observer. In this case, eq.(3) can be reduced to:

$$\frac{D_a^{fit}}{D_a^{true}} = \left(\frac{T^{true}}{T^{fit}}\right)^2 \frac{\Lambda(x^{as}, z^{fit}, T^{fit})}{\Lambda(x^{true}, z^{true}, T^{true})} \approx \frac{\Lambda^{as}}{\Lambda^{true}}, \qquad (4)$$

where T^{true} and x^{true}, z^{true} are the true temperature and abundances of the gas, T^{fit} and z^{fit} are the corresponding best-fit values obtained from X-ray spectral fitting and x^{as} is the assumed helium abundance and D_a^{fit} is the angular distance inferred from the analysis.

For hydrogen–helium plasma ($z = 0$), the cooling function is given by:

$$\Lambda(x, z = 0, T) = \epsilon_{ep}(T)\ \frac{1 + 4x\, g_{ff}(Z_{He})/g_{ff}(Z_H)}{1 + 2x}, \qquad (5)$$

where $\epsilon_{ep}(T)$ is the bremsstrahlung emissivity for a pure electron-proton plasma, $x = n_{He}/n_H$ is the helium abundance by the number of particles with respect to hydrogen and $g_{ff}(Z)$ is the frequency-averaged Gaunt-factor for the element with charge Z. The relative error in the distance determined from equation (4) is then

$$\frac{D_a^{fit}}{D_a^{true}} = \left(\frac{T^{true}}{T^{fit}}\right)^2 \frac{1 + 4\tilde{g}\, x^{as}}{1 + 4\tilde{g}\, x^{true}} \frac{1 + 2x^{true}}{1 + 2x^{as}}. \qquad (6)$$

where $\tilde{g} \equiv g_{ff}(Z_{He})/g_{ff}(Z_H)$. If we neglect the weak dependence of the Gaunt-factor on Z (Hummer 1988) and the related weak temperature bias (see Fig. 1), we can simplify the above expression as follows:

$$\frac{D_a^{fit}}{D_a^{true}} \approx \frac{1 + 4x^{as}}{1 + 4x^{true}} \frac{1 + 2x^{true}}{1 + 2x^{as}}, \qquad (7)$$

This approximation was previously derived by Markevitch (2007). The distance bias described by equations (6) and (7) is shown in Fig. 2. We see that the difference between equations (6) and (7) is small.

If the gas contains heavy elements, the dependence of the distance bias on x^{as} becomes more complicated. The heavy elements contribute to the total X-ray luminosity by continuum emission (recombination, bremsstrahlung, 2-photon emission) and line emission. As was shown in Section 2.1, for $x^{as} \neq x^{true}$, bias also appears in measuring the heavy element abundances. Hence, there is an additional bias in D_a^{fit} due to the incorrectly accounted contribution of heavy elements to Λ in equation (3).

To investigate this quantitatively, we used the results of simulations performed in Section 2.1. From the best-fit values of temperature and metal abundances obtained there, we computed the cooling function Λ^{as} in eq.(4) and the ratio D_a^{fit}/D_a^{true}. The result is shown in Fig. 2. Replacing the Chandra response with that of XMM-Newton yields practically the same results.

As can be seen from Fig. 2, for helium–hydrogen plasma there is no significant difference between the accurate eq.(6) and approximate eq. (7). However, these formulae underestimate the effect for a plasma of solar abundance by ≈ 5–10%, the difference becoming larger at lower temperatures.

3 REDISTRIBUTION OF HELIUM AND HEAVY ELEMENTS BY DIFFUSION IN CLUSTERS OF GALAXIES

The element abundance distribution in the ICM is determined by a number of physical processes. The initial composition of the ICM will change with time due to ejection of heavy elements by supernovae, turbulent mixing and diffusion in the gas. The role of diffusion in shaping ICM abundance profiles has been disputed for a long time. As is well known, transport processes in the ICM may be supressed by magnetic fields (e.g. Gilfanov & Sunyaev 1984; Ettori & Fabian 2000; Markevitch et al. 2003; Komarov et al. 2013). However, the chaotic fluctuations of the magnetic field produced by turbulence can make the large scale transport coefficients big enough to make the diffusion important

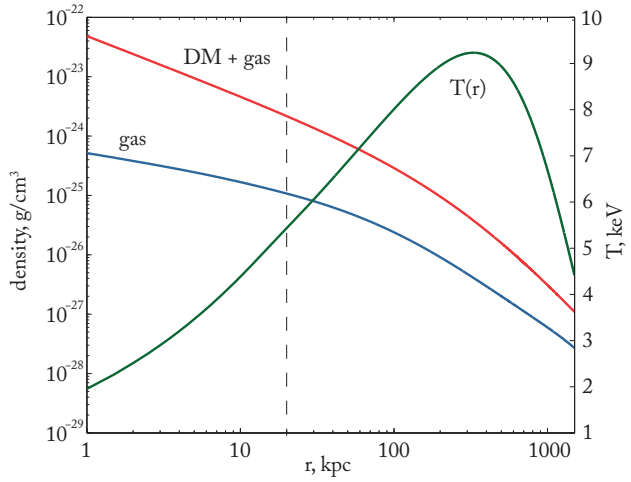

Figure 3. The profiles of the ICM density (blue), temperature (green) and total mass density (red) in Abell 2029 that were used in the diffusion calculations. For the temperature profile, we combined the models of (Vikhlinin et al. 2006) and (Lewis et al. 2002) outside and inside 20 kpc (vertical dotted line), respectively. The radius of 20 kpc corresponds to about 14″.

(Narayan & Medvedev 2001). On the other hand, turbulent mixing can counteract diffusion, its effect on the distribution of elements depending on the turbulence spatial scale and velocity (Ascasibar & Markevitch 2006).

We considered the problem of diffusion of elements in the ICM in full detail but ignored the complexity introduced by the magnetic fields, turbulent mixing and enrichment of the ICM by supernovae. The goal of this exercise was to estimate the maximal effect that diffusion can have on various cosmologically important measurements with clusters of galaxies.

3.1 Calculation method

Diffusion of elements is driven by the force of gravity and by density and temperature gradients. Density gradients tend to restore a homogeneous distribution of the element abundances in plasma, whereas gravitational sedimentation tends to concentrate plasma's heavy particles to the cluster center; the equilibrium state distribution of elements of mass m_i is proportional to the Boltzmann factor $n \sim e^{-m_i\phi(r)/kT}$, where ϕ is the gravitational potential (Gilfanov & Sunyaev 1984; Chuzhoy & Loeb 2004; Abramopoulos, Chanan & Ku 1981). The presence of temperature gradients in plasma gives rise to thermal diffusion, which tends to remove heavy and more highly charged particles from colder regions (Burgers 1969; Chapman & Cowling 1970; Monchick & Mason 1985; Shtykovskiy & Gilfanov 2010).

To take into account all these processes, we considered a full diffusion problem by solving the system of Burger's equations (Burgers 1969). We used the numerical scheme from Shtykovskiy & Gilfanov (2010); the interested reader is referred to that paper for the details. Here we describe the main simplifying assumptions:

(i) We consider a 4-component plasma consisting of hydrogen, helium, a heavy element ($\mathcal{A}$, Z) and electrons. The hydrogen and helium are assumed to be fully ionized. In all of the calculations presented here, the heavy element is Fe^{+24}. As was demonstrated in Shtykovskiy & Gilfanov (2010), adding other heavy ions does not lead to noticeable differences in the diffusion picture, moreover, distributions of all metals change in an approximately identical manner.

(ii) We use a spherical model of a cluster in hydrostatic equilibrium. Because of the non-negligible helium abundance, diffusion changes the total pressure: $p = \Sigma n k_b T$, hence hydrostatic equilibrium is violated and a net flow of particles appears. However, because the sound speed in the ICM is much higher than the diffusion velocity, hydrostatic equilibrium restores quickly and stationary Burger's equations remain valid. The (small) net flow velocity is calculated using the Euler equation.

(iii) All velocities, temperature and density gradients are required to vanish at the inner point $r = 0$. At the outer boundary, a constant density boundary condition is set. This is equivalent to assuming that the galaxy cluster is imbedded in an infinite reservoir of gas. In our baseline model, the cluster outer boundary is located at a distance of 1500 kpc from the cluster center. We have verified that the solution in the inner regions of the cluster is insensitive to this condition (see also Shtykovskiy & Gilfanov 2010). Furthermore, we also considered the case of an opaque boundary condition by setting the speeds of all species equal to zero at the outer boundary. The resulting solution at $t = 7$ Gyr differs by less than a few per cent from the solution for our default boundary conditions almost everywhere out to a radial distance of ~ 1000 kpc.

(iv) The evolution of the temperature profile is not self-consistently included in the calculations. The temperature profile is fixed, $T(r, t) = T(r, 0)$, and heat transport in the plasma is switched off, i.e. there is no heat flux term in our equations. This is equivalent to assuming that heat transport and the activity of the central AGN are fully compensated by the radiative cooling of gas. The possibility of a stable configuration of this type has been demonstrated e.g. in Guo, Oh & Ruszkowski (2008).

3.2 Cluster models

We conducted our calculations for cool-core and isothermal cluster models. To build the cool-core cluster model, we use data for the A2029 cluster of galaxies. This cluster, located at $z = 0.0767$, is known to have regular X-ray morphology and has been studied extensively in X-rays with ROSAT (Sarazin et al. 1998), Chandra (Lewis et al. 2002; Vikhlinin et al. 2005, 2006) and XMM-Newton (Snowden et al. 2008).

We use the best-fit model from Vikhlinin et al. (2006) to describe the temperature profile of A2029. This model is defined outside of 20 kpc from the cluster center. To continue the temperature profile inward of 20 kpc, we use the best-fit model from Lewis et al. (2002), which is defined down to 1 kpc from the cluster center. We smoothly stitched the two models at 20 kpc using a 5-degree polynomial. Within 1 kpc of the cluster center, we extrapolated the temperature profile using a 3-degree polynomial with a vanishing derivative in the cluster center. The central temperature is fixed at 2 keV.

For the total mass, we use a NFW (Navarro, Frenk & White 1997) profile

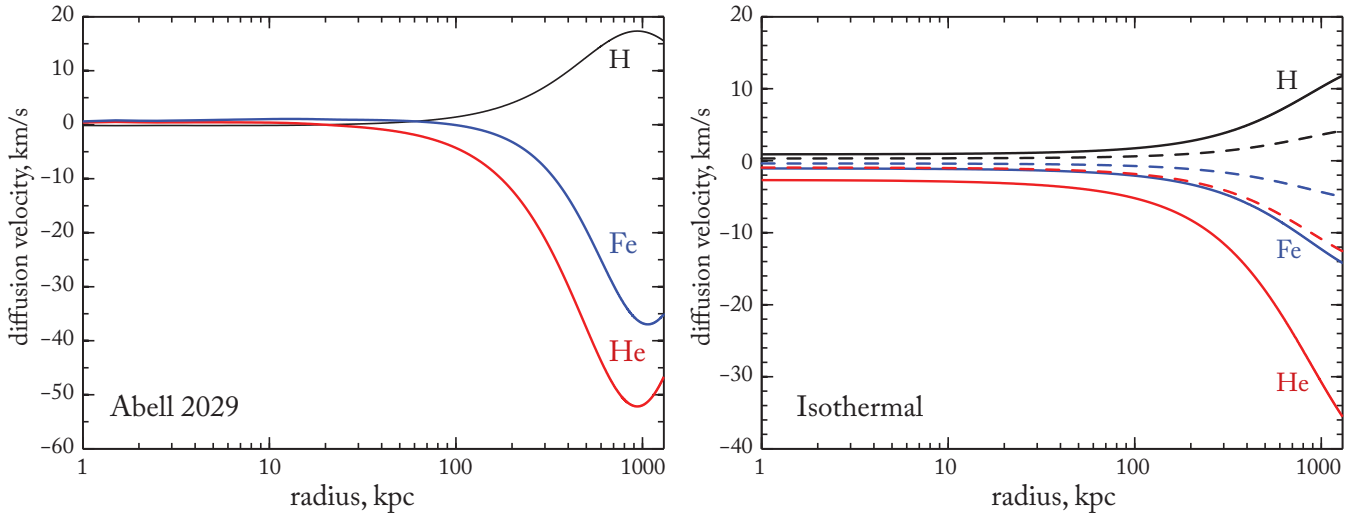

Figure 4. The initial diffusion velocity of H^+ (black), He^{+2} (red) and Fe^{+24} (blue). Positive velocity corresponds to outward flow. The left panel shows the results for A2029 and the right panel for an isothermal cluster with a temperature of 3 (dashed line) and 6 (solid line) keV. The mass profiles of the isothermal clusters are the same as for A2029.

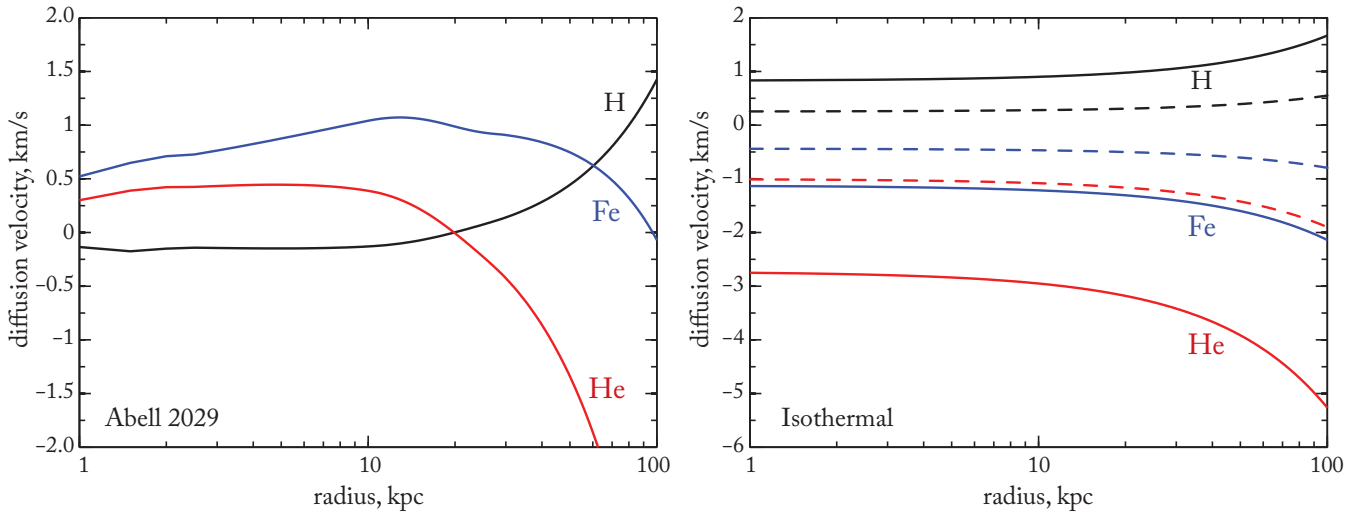

Figure 5. Same as Fig. 4, but for the central parts of the clusters.

$$\rho = \frac{\rho_s}{r/r_s(1+r/r_s)^2}, \tag{8}$$

with $r_s = 337$ kpc (Vikhlinin et al. 2006). The normalization value, $\rho_s = 1.7 \times 10^{-25}$ g/cm^3, was determined using the best-fit gas density profile from Vikhlinin et al. (2006), the aforementioned temperature profile and the condition of hydrostatic equilibrium, $\frac{\Delta p}{\rho} = -g$. Using the temperature profile, the normalized NFW profile and the condition of hydrostatic equilibrium, we finally determined the gas density distribution. The resulting profile is close to that from Vikhlinin et al. (2006). The gas mass fraction is 15% inside $r_{500} = 1360$ kpc (recall that the outer boundary is fixed at 1500 kpc). The final profiles of the total mass density, gas density and temperature are shown in Fig. 3.

For the isothermal cluster models, we assume the same dark matter distribution as in A2029. We considered two isothermal models with temperatures of 3 and 6 keV. Similar to the cool-core model, the gas density distribution was calculated assuming hydrostatic equilibrium. The gas mass fraction in these models is also 15%. The isothermal cluster models allow us to isolate the effect of thermal diffusion, effectively switching it off in Burger's equations.

In all the considered cluster models, the mean free path for protons at the outer radius is $\sim$ 10–20 kpc, hence the diffusion approximation is valid over the entire cluster.

3.3 Evolution of element abundance profiles

We start our calculations with the solar mass fractions of 0.75, 0.25, $1.8 \cdot 10^{-3}$ for H, He and Fe, respectively (Anders & Grevesse 1989). The initial abundance profiles are assumed to be flat. The initial profiles of the diffusion velocity of H^+, He^{+2} and Fe^{+24} for A2029 and the isothermal cluster are shown in Fig. 4; Fig. 5 zooms in on the

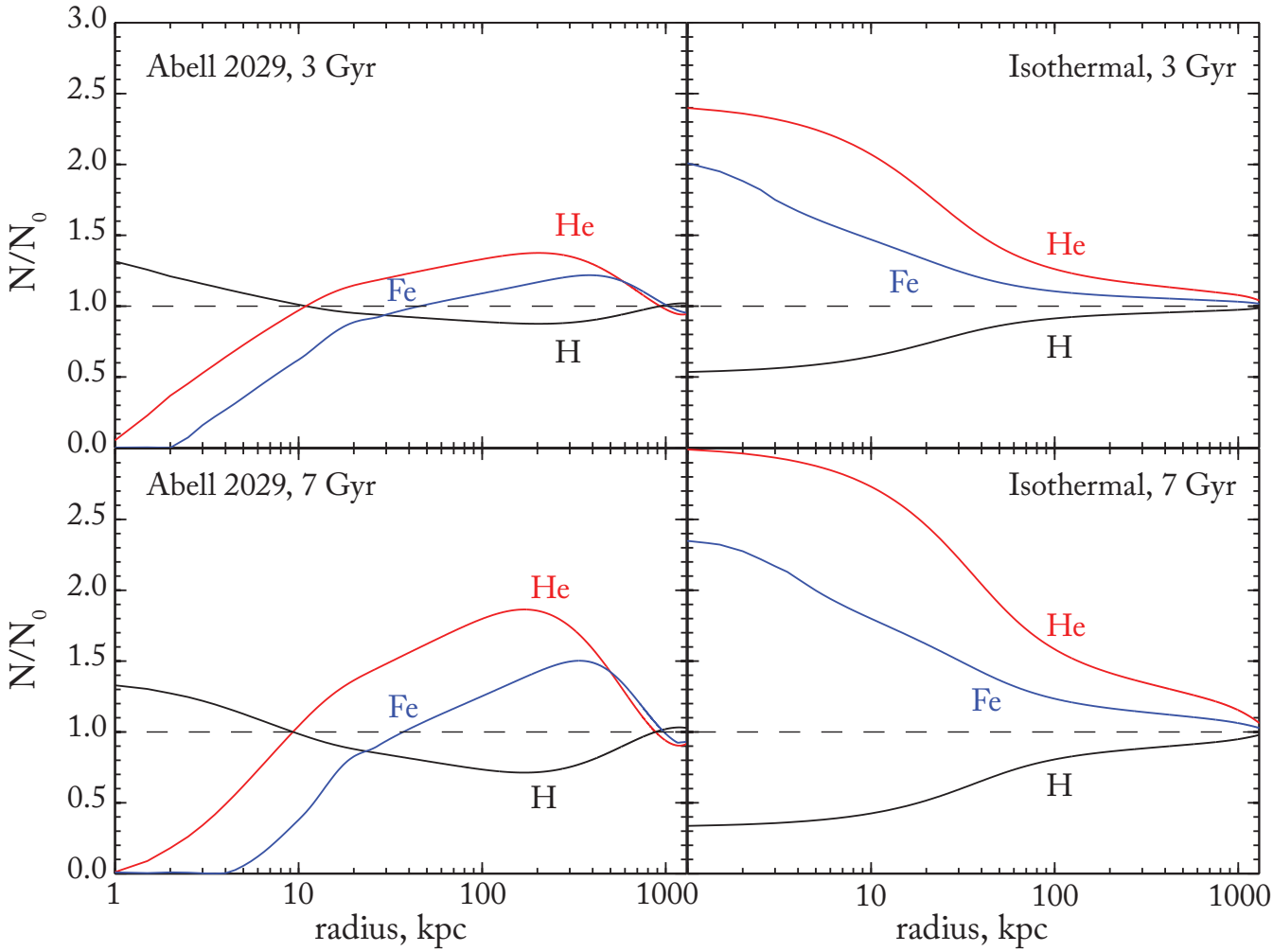

Figure 6. Element distributions after 3 (top panels) and 7 (bottom panels) Gyr of diffusion, normalized to the respective distributions at $t = 0$. Hydrogen, helium and iton are shown the black, red and blue lines, respectively. The left panels are for A2029 and the right panels are for an isothermal cluster with $kT = 6$ keV and the same dark matter distribution as in A2029.

velocities in the central part of the cluster. Positive velocity corresponds to outflow and negative to inflow.

In the central 20 kpc region of A2029, helium and iron have positive velocities and only hydrogen flows towards the cluster center. Such behavior is caused by the large temperature gradient in the central part of the cluster (from the center to $\sim$ 300 kpc, Fig. 3). Thermal diffusion tends to evacuate heavy elements from the cool core, counteracting gravity. On the other hand, the outward decrease of temperature beyond $r > 500$ kpc acts in the same direction as gravitational sedimentation and increases the diffusion velocity as compared to isothermal cluster models.

Fig. 6 shows the accumulated effect of the diffusion after 3 and 7 Gyr. After 7 Gyrs, the thermal diffusion completely removes iron from the central part of A2029. The same is true for helium, albeit to somewhat lesser extent. The combined effect of gravitational sedimentation and thermal diffusion increases the concentration of both elements at $\sim$ 100–200 kpc from the cluster center. The hydrogen distribution changes in the opposite sense, in order to keep hydrostatic equilibrium. As a result, complex abundance distributions of elements are formed. The particular shape of these distributions is determined by the detailed shape of the temperature profile, as the net diffusion velocity depends on the amplitude of the temperature gradients. Although the temperature profiles vary significantly from cluster to cluster, a picture qualitatively similar to that for A2029 arises for other cool-core clusters: the abundance of elements heavier than hydrogen is suppressed in the cluster center and peaks at intermediate radii, $\sim$ few hundred kpc, due to the combined effect of thermal diffusion and gravitational separation (see Shtykovskiy & Gilfanov (2010) for a few other examples).

For the isothermal cluster model, the gravitational sedimentation modifies the element distributions in a more monotonic fashion, increasing their concentrations towards the cluster center. As demonstrated in previous work (Gilfanov & Sunyaev 1984; Chuzhoy & Loeb 2004), the enhancement is most significant for helium and is somewhat smaller for iron and other metals. In particular, the helium concentration in the cluster center can increase by up to a factor of $\approx$ 2.4–3 after 3–7 Gyrs. Because of the factor of

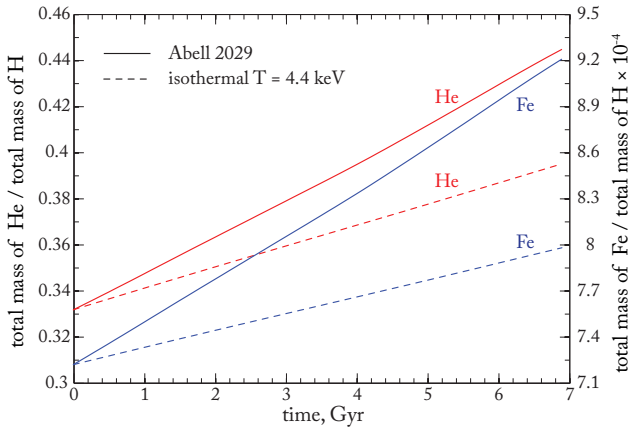

Figure 7. Evolution of the cluster averaged abundances, by mass, of helium (red lines) and iron (blue lines) as a function of time for A2029 (solid lines) and isothermal cluster with the temperature equal to the outer temperature of the A2029 model ($T = 4.4$ keV) (dashed lines).

$\sim$ 2–3 decrease of the hydrogen concentration in the center, the increase in the helium abundance is larger and can achieve a factor of $\sim$ 5–9. As the diffusion velocity depends on temperature as $v \propto T^{3/2}$, the effect is stronger for higher temperature clusters.

3.4 Outflow and inflow of particles through the cluster outer boundary

Both theory and cosmological simulations predict that the temperature profiles of clusters are approximately self-similar (for a detailed discussion see, e.g., Katz & White 1993; Loken et al. 2002; Bryan & Norman 1998). This prediction is confirmed by observations (e.g. Vikhlinin et al. 2005). A prominent feature of the predicted and observed temperature profiles is that the ICM temperature decreases outwards in the outer regions of clusters, beyond several hundred kpc. As was demonstrated in the previous sections, the combined effect of gravitation sedimentation and thermal diffusion will lead to inflow of elements heavier than hydrogen and outflow of hydrogen through the outer boundary of the cluster of galaxies. This will result in a long-term increase of the cluster-averaged abundances of elements heavier than hydrogen. Below, we calculate the net flux of particles through the outer boundary in order to evaluate the amplitude of this effect. Recall that in our standard A2029 model, $r_{out} = 1.5$ Mpc.

In our cool-core cluster model, the ICM mass inside r_{out} obtained by integrating ρ_g (Fig. 3) is 1.4×10^{14} $M_\odot$. At $t = 0$, the hydrogen, helium and iron mass fractions take their solar values of 0.75, 0.25 and 1.8×10^{-3}, respectively, and the corresponding diffusion velocities at the outer boundary are $v_H = +13.8$, $v_{He} = -41.2$ and $v_{Fe} = -31.8$ km s^{-1} (Fig. 4). Hence, the initial mass flow rates are $q_H = -1190$, $q_{He} = 1185$ and $q_{Fe} = 5$ $M_\odot$/year, where positive sign means that the total mass of the given element in the cluster is increasing. Thus, at the time $t = 0$ the abundances will be increasing at rates of:

$$\dot{A}_{He}/A_{He} \approx 4.8 \cdot 10^{-2} \text{ Gyr}^{-1} \quad (9)$$

$$\dot{A}_{Fe}/A_{Fe} \approx 3.9 \cdot 10^{-2} \text{ Gyr}^{-1} \quad (10)$$

In the isothermal cluster model, these rates are correspondingly smaller.

The detailed long-term evolution of the cluster-averaged abundances computed from results of our numerical calculations is shown in Fig. 7. After 7 Gyr, 4.5% of the hydrogen initially present in the cluster will have outflown through the outer boundary, whereas the total masses of helium and iron in the ICM will have increased by 28% and 22%, respectively. This will result in an increase of their cluster-averaged abundances by 33% and 27%, respectively. For the isothermal cluster ($T = 4.4$ keV), the cluster-averaged abundances of helium and iron will have increased by 19 and 11%, respectively, after 7 Gyr. Due to outflow of hydrogen and inflow of helium and heavier elements through the outer boundary of the cluster, the mean molecular weight of the ICM increases with time. We note that due to our assumption of hydrostatic equilibrium at $t = 0$, there is no net mass flow through the outer boundary at the initial moment. Once diffusion starts to operate, the total pressure changes and the gas is pushed out of the equilibrium which is restored via net gas motion. As a result, there is net inflow of mass through the outer boundary and the total mass of the ICM increases at the average rate of $\sim 0.5\%$ per Gyr.

We conclude that the cluster-averaged abundances of helium and metals can significantly increase due to the combined effect of thermal diffusion and gravitational sedimentation at the outer boundary of the cluster, provided that these elements are present in sufficient amounts in the intergalactic medium (IGM), outside this boundary. In the above calculations we assumed that their abundances are solar in the IGM. This is true for helium, but metals are not expected to be present in significant amounts outside clusters of galaxies. Therefore, eq.(10) may strongly overestimate the effect for iron. We finally note that the topology of the magnetic field and characteristics of turbulence may be different in the central parts of clusters of galaxies and in their outskirts. Therefore, diffusion may be suppressed in the center of the cluster but operate at sufficient strength in its outer regions and vice versa.

4 EFFECT OF DIFFUSION ON THE INTERPRETATION OF X-RAY AND SZ DATA

Thermal diffusion can thus significantly affect the distribution of helium and heavy elements in galaxy clusters. This, together with the bias in the determination of heavy element abundances introduced by the standard assumption of solar helium abundance (Section 2), can have important consequences for the interpretation of X-ray and SZ observations of clusters. We now use results of previous sections to estimate the expected biases in the determination of cluster parameters.

We divided the model cluster into concentric spherical shells and generated the X-ray spectrum of emission from each shell using the APEC model in XSPEC and the electron number density, temperature and element abundances resulting from the diffusion calculations in Section 3.3. We then fitted the generated spectra by APEC assuming the solar abundance of helium. The results are shown in Fig. 8. In

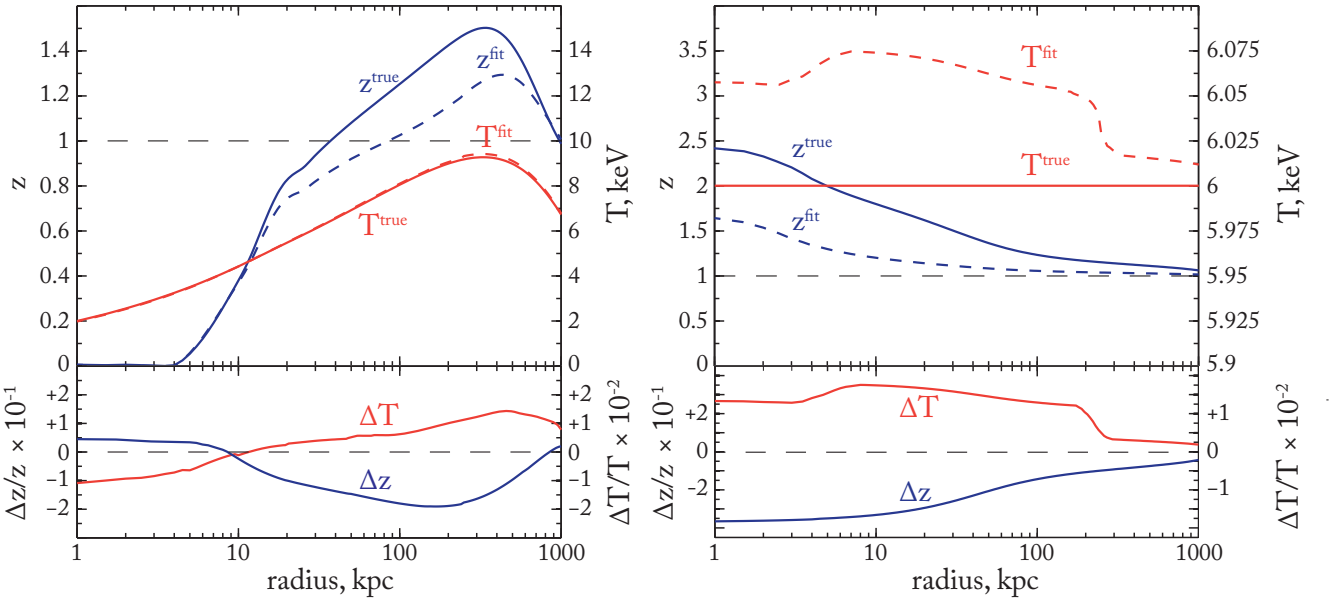

Figure 8. Abundance and temperature biases in X-ray spectral analysis for A2029 (*left*) and for an isothermal cluster with $kT = 6$ keV (*right*) at $t = 7$ Gyr (cf. Fig. 6). *Top:* The blue solid line shows the true metal abundance, while the blue dashed line shows its best-fit value obtained under the assumption of solar helium abundance. The corresponding red lines show the true and best-fit temperature profiles. *Bottom:* The relative error in the metal abundance (blue) and temperature (red) determination.

the top panel, we compare the true radial profiles of metal abundance and temperature with those determined from the fits. Their fractional difference is shown in the bottom panel; it illustrates the bias in the determination of ICM parameters from X-ray spectroscopy. These results are presented for spherical shells, rather than for projected quantities, i.e. we implicitly assume that the X-ray data are of sufficient quality to enable the de-projection analysis.

We see that the assumption of solar helium abundance results in a significant, up to $\approx$ 20–35% bias in the metal abundance determination. For the isothermal cluster it leads to a significant, more than a factor of ~ 2, underestimate of the effect of the gravitational sedimentation for metals. The total mass of heavy elements in the ICM is underestimated by 5.7% and 5.5% for A2029 and the isothermal cluster, respectively. The total mass of gas is underestimated by 7% and 8%, respectively. On the other hand, the temperature is only weakly sensitive to the helium abundance assumption and bias in its determination is thus small.

The redistribution of elements in the ICM also modifies the electron density profile (due to the electroneutrlity condition) and consequently the amplitude of the SZ effect. In the left panel of Fig. 9, we show the change in the radial profile of electron density after 7 Gyr of diffusion for the isothermal cluster with $kT = 6$ keV and for A2029. Comparison with Figs. 6 and 9 indicates that the change in the electron density is primarily caused by the diffusion of hydrogen. In the right panel of Fig. 9, we show the resulting changes in the Comptonization parameter as a function of the projected radius.

We can finally estimate the bias in the determination of the angular distance, using equation (3). To this end, we again assume that the observer has performed a de-projection analysis of the X-ray data and determined the temperature, metal abundance(s) and emission measure for each spherical shell. We replace the integral in equation (3) by a sum over spherical shells. We find that the assumption of solar He abundance leads to an underestimate of the angular distance by $\approx$ 13% and $\approx$ 15% for the cool-core and isothermal cluster models respectively, at $t = 7$ Gyr and using the 1500 kpc aperture. The bias increases almost linearly with time and weakly depends on the aperture for apertures exceeding ~ 0.5 Mpc in radius. Its detailed dependence on time and aperture are shown in Fig. 10.

5 SUMMARY

We have considered the role of abundance anomalies in the intra-cluster medium in interpretating X-ray and microwave observations of clusters of galaxies in the cosmological context. In particular, we investigated the role of diffusion of elements in the ICM. As is well-known (Gilfanov & Sunyaev 1984; Chuzhoy & Nusser 2003; Chuzhoy & Loeb 2004; Ettori & Fabian 2006; Shtykovskiy & Gilfanov 2010), it is the density distribution of helium which can be affected by gravitational sedimentation of elements most strongly. However, since helium is fully ionized in the ICM, its abundance (to the contrary to metal abundances) cannot be directly measured from equivalent widths of emission lines. Therefore, in practice, it is usually assumed that helium abundance in the ICM equals to its primordial value. Should this assumption be incorrect, significant biases in estimating the metal abundances, emission measure and total mass of the gas may arise (Section 2; see also Drake 1998; Ettori & Fabian 2006).

The role of diffusion in the ICM of clusters of galaxies is still debated. The two well-known factors that can potentially significantly reduce its importance are magnetic fields and the mixing effect of large-scale turbulence. We

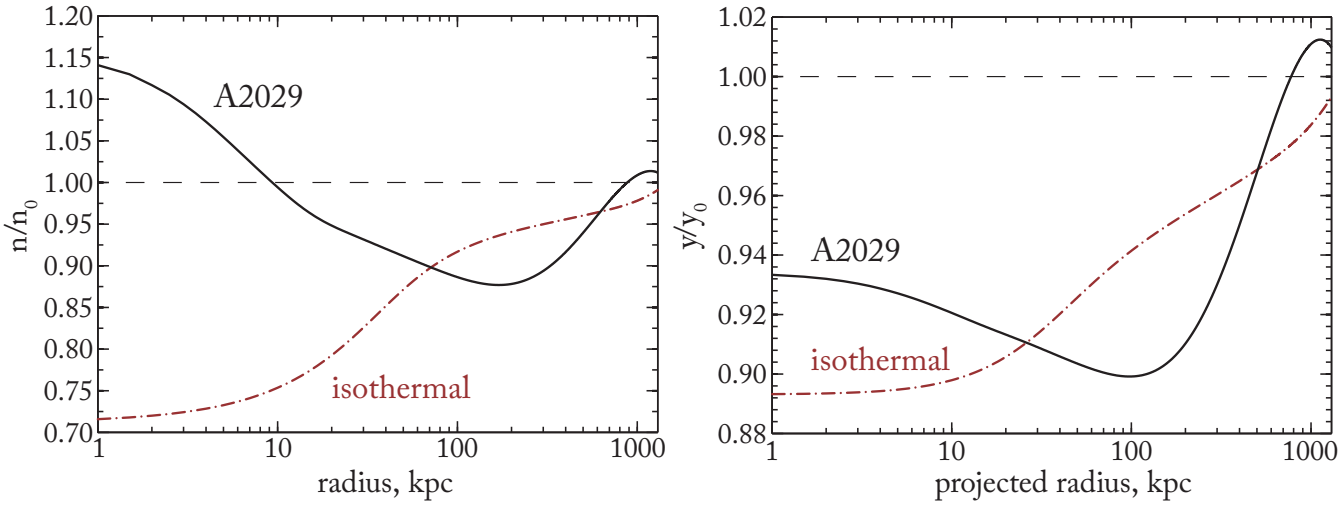

Figure 9. *Left:* The change in the radial profile of electron density after 7 Gyr of diffusion for A2029 (black line) and for the isothermal cluster with $kT = 6$ keV (red line) as a function of the radial distance to the cluster center. *Right:* The corresponding change in the Comptonization parameter, i.e. of the amplitude of the SZ-effect, as a function of projected radius.

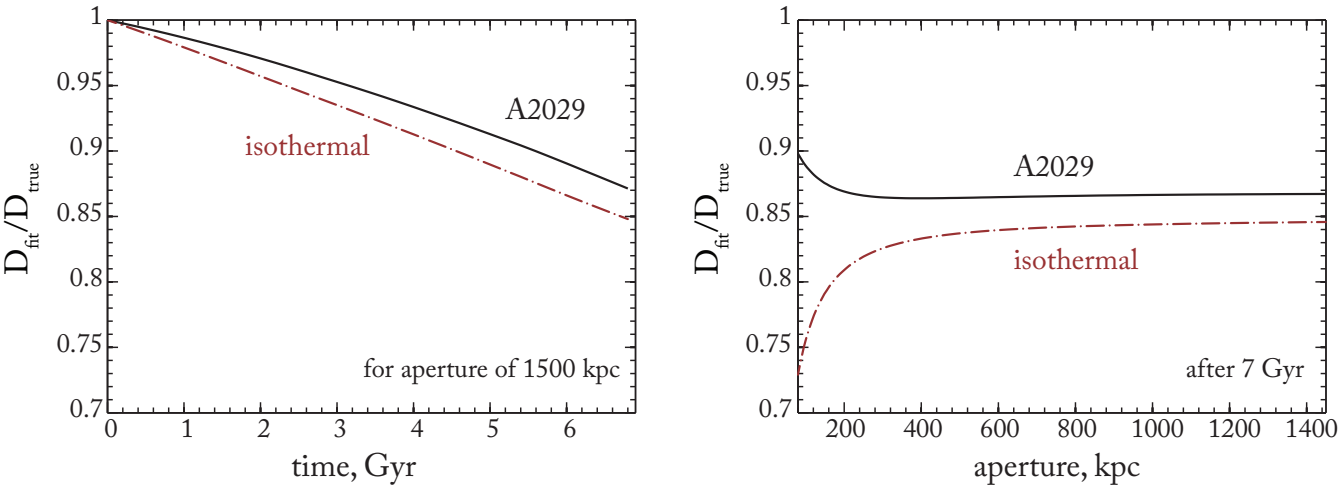

Figure 10. The bias in the angular distance determined from the combined analysis of SZ and X-ray data. The black lines show results for a cool-core cluster, the red lines are for the isothermal cluster. The distance bias is shown as a function of time for an aperture of 1500 kpc (*left panel*) and as a function of aperture at $t = 7$ Gyr (*right panel*).

ignored this complexity and investigated the maximum possible effect of diffusion on the cosmological measurements with clusters of galaxies. To this end, we considered the full set of Burger's equations for a multi-component plasma and solved them for two cluster models: (i) a cool-core cluster, which was represented by the temperature and mass profiles of A2029, and (ii) an isothermal cluster with the same mass distribution and temperature of $T = 3$ and 6 keV. In the case of the isothermal cluster, canonical gravitational sedimentation of elements occurs leading to a factor of $\sim$ 5–10 enhancement of helium and metal abundances in the cluster center on a $\sim$ 3–7 Gyr time scale. In the case of the cool-core cluster model however, thermal diffusion counteracts the gravitational sedimentation, significantly reducing the abundances of all elements heavier than hydrogen in the cluster inner core, $r \leqslant$ 10–20 kpc and producing an up to a factor of $\sim$ 1.5–2 enhancement of their abundances at the intermediate radii $\sim$ 100–500 kpc.

There is a significant flux of helium and metals and outflow of hydrogen through the outer boundary of the cluster. This will lead to a noticeable increase in the cluster averaged abundances of the elements heavier than hydrogen at a rate of $\sim$ 5% per Gyr. Of course, for the metals, this depends on their actual abundance in the IGM.

Such a significant redistribution of elements will lead to a number of biases in the cluster parameters determined from X-ray data. The key role in these biases is played by an incorrect assumption about the helium abundance. In particular, the metal abundances can be underestimated by up to $\approx$ 10–40% and the total gas mass can be underestimated by $\approx$ 7%. When X-ray data are combined with microwave measurements to measure the angular distance to clusters of galaxies, the diffusion of elements can lead to an underes-

timate of the latter by $\sim$ 10–15% for apertures of the order r_{500}, with the effect being stronger for isothermal clusters. Furthermore, in the case of an isothermal cluster with temperature $kT = 6$ keV, the effect can reach $\approx$ 20–25% for small apertures of $\sim$ 100–200 kpc.

REFERENCES

Abramopoulos, F., Chanan, G., Ku, W., ApJ, 1981, 248, 429

Anders, E., Grevesse, N., Geochimica et Cosmochimica Acta, 1989, 53, 197

Arnaud, K., Astronomical Data Analysis Software and Systems V, eds. Jacoby G. and Barnes J., 1996, ASP Conf. 101, 17

Ascasibar, Y., Markevitch, M., ApJ, 2006, 650, 102

Bonamente, M., Joy, M., LaRoque, S., Carlstrom, J., Reese, E., Dawson, K., ApJ, 2006, 647, 25

Bryan, G., Norman, M., ApJ, 1998, 495, 80

Bulbul, G. E., Hasler, N., Bonamente, M., Joy, M., Marrone, D., Miller, A., Mroczkowski, T., A&A, 2011, 533, A6

Burgers, J. M., Flow Equation for Composite Gases. New York: Academic Press., 1969

Carlstrom, J. E., Holder, G. P., Reese, E. D., ARA&A, 2002, 40, 643

Chapman, S., Cowling, T., The mathematical theory of non-uniform gases. Cambridge: University Press, 1970.

Chuzhoy, L., Nusser, A., MNRAS, 2003, 342, L5

Chuzhoy, L., Loeb, A. MNRAS, 2004, 349, L13

Drake, J., ApJ, 1998, 496, L33

Ettori, S., Fabian, A. C., MNRAS, 2000, 317, L57

Ettori, S., Fabian, A. C., ApJ, 2006, 369, L42

Fabian, A. C., Pringle, J. E., MNRAS, 1977, 181, 5P

Fabian, A. C., Annual Review of Astronomy and Astrophysics, 1994, 32, 277

Guo, F., Oh, S. P., Ruszkowski, M., ApJ, 2008, 688, 859

Gilfanov, M. R., Syunyaev, R. A. Pisma v Astronomicheskii Zhurnal, 1984, 10, 329

Hummer, D., ApJ, 1988, 327, 477

Katz, N., White, S., ApJ, 1993, 412, 455

Kneller, J., Steigman, G., New Journal of Physics, 2004, 6, 117

Komarov, S., Churazov, E., Schekochihin, A., eprint arXiv:1304.1857, 2013

Kravtsov, A. V., Vikhlinin, A., Nagai, D.., ApJ, 2006, 650, 128

Lewis, A. D. and Buote, D. A. and Stocke, J. T., ApJ, 2002, 34, 1207

Loken, C., Norman, M., Nelson, E., Burns, J., Bryan, G., Motl, P., ApJ, 2002, 579, 571

Markevitch, M., Vikhlinin, A. Physics Reports, 2007, 443, 1

Markevitch, M., eprint arXiv:0705.3289, 2007

Markevitch et al., ApJ, 2003, 586, L19

Monchick, L., Mason, E., Physics of Fluids, 1985, 28, 3341

Motl, P. M., Hallman, E. J., Burns, J. O., Norman, M. L., ApJ, 2005, 623, L63

Narayan, R., Medvedev, M. V., ApJ, 2001, 562, L129

Navarro, J. F., Frenk, C. S., White, S. D. M. ApJ, 1997, 490, 493

Planck Collaboration, et al., arXiv, 2012, arXiv: 1208.3611

Planck Collaboration, et al., arXiv, 2013, arXiv: 1303.5089

Plagge T., et al., ApJ, 2010, 716, 1118

Plagge T., et al., arXiv, 2012, arXiv: 1203.2175

Reese E. D., et al., ApJ, 2012, 751, 12

Sarazin, C. L., Wise, M. W., Markevitch, M. L., ApJ, 1998, 498, 606

Shtykovskiy, P., Gilfanov, M., MNRAS, 2010, 401, 1360

Silk, J., White, S. D. M., ApJ, 1978, 226, L103

Smith, R. K., Brickhouse, N. S., Liedahl, D. A., Raymond, J. C., ApJ, 2001, 556, L91

Snowden, S. L., Mushotzky, R. F., Kuntz, K. D., Davis, D. S., A&A., 2008, 478, 615

Sunyaev, R. A., Zeldovich, Y. B., Comments on Astrophysics and Space Physics, 1972, 4, 173

Sunyaev, R. A., Zeldovich, Y. B., ARA&A, 1980, 18, 537

Vikhlinin, A., Markevitch, M., Murray, S. S., Jones, C., Forman, W., Van Speybroeck, L., ApJ, 2005, 628, 655

Vikhlinin, A., Kravtsov, A., Forman, W., Jones, C., Markevitch, M., Murray, S. S., Van Speybroeck, L., ApJ, 2006, 640, 691

Walker, T., Steigman, G., Kang, H.., Schramm, D., Olive, K., ApJ, 1991, 376, 51